ECS Transactions, 16 (5) 471-478 (2008)
10.1149/1.2981628 ©The Electrochemical Society

Effects of Low Temperature O_2 Treatment on the Electrical Properties of Amorphous $LaAlO_3$ Films Made by Atomic Layer Deposition

Y. Liu[a], H. Kim[a], J.-J. Wang[a], H. Li[b], and R. G. Gordon[a]

[a] Department of Chemistry, Harvard University, Cambridge, Massachusetts 02138, USA
[b] Rohm and Haas Electronic Materials LLC, North Andover, Massachusetts 01845, USA

Amorphous $LaAlO_3$ films were deposited on hydrogen-terminated silicon substrates by atomic layer deposition (ALD) at 300 ^oC. The precursors were lanthanum tris(*N,N'*-diisopropylformamidinate), trimethylaluminum (TMA) and water. Capacitance-voltage measurements made on ALD MoN/$LaAlO_3$/Si stacks showed humps especially at low frequencies. They were effectively removed by O_2 treatment at 300 ^oC without affecting the dielectric constant (κ~15). The O_2 treatment can be carried out either after deposition of a $LaAlO_3$ film, or after each ALD cycle. The O_2 treatment also lowered the leakage current from 80 mA cm^{-2} to 1 mA cm^{-2} for EOT = 1.3 nm. This indicates that oxygen vacancies are the main defects in as-deposited $LaAlO_3$. Oxygen treated $LaAlO_3$ is one of the best candidates for future high-κ dielectric material due to its low leakage, low defect density and abrupt interface with silicon.

Introduction

Since the introduction of metal oxide semiconductor (MOS) field-effect transistors (FETs) as the centerpiece of microelectronic devices, scaling down of transistor size has continued to improve transistor performance. Therefore, the thickness of SiO_2-based gate dielectrics has been scaled down to keep the transistor drive current high enough to sustain speed enhancement. The thickness for gate dielectric layers specified in the ITRS roadmap has become so small that the leakage current density would be too high if SiO_2-based films were used as gate dielectrics (1). One solution for this problem is the integration of high-κ dielectrics into gate stacks. Recent developments in employing high-κ dielectric layers have focused on hafnium-based dielectrics. However the requirement of a significantly thick (>0.5 nm) SiO_2 interlayer or a formation of low-dielectric-constant silicate alloys with SiO_2 limits future scalability of Hf-based dielectrics (2).

$LaAlO_3$ has been considered as a potential high-κ dielectric. It has a high dielectric constant (κ_{bulk} is 20-25) (3, 4) as compared to SiO_2 (κ~3.9), wide band gap (E_g=5.8 eV), high band offsets with respect to silicon (>2 eV) (5, 6) and abrupt interfaces when grown on silicon (7, 8). Many studies have shown that it is thermally stable in contact with silicon up to ~ 800 ^oC (9-12). Amorphous $LaAlO_3$ films have been grown using several physical and chemical deposition methods such as molecular beam deposition (MBD) (9, 13), sputtering (10, 11), electron-beam evaporation (14), chemical vapor deposition (CVD) (15) and atomic layer deposition (ALD) (16). ALD is a very attractive method for depositing DRAM insulators and advanced gate oxides for 3-D transistors, because the film thickness is easy to control, and the uniformity across the wafer and deep trenches is

Downloaded 06 Feb 2009 to 128.103.93.158. Redistribution subject to ECS license or copyright; see http://www.ecsdl.org/terms_use.jsp

better than with other deposition methods. Many issues, including high leakage current and high densities of bulk traps, remain to be resolved. Thus, in this letter, we suggest O_2 annealing during or after $LaAlO_3$ deposition to decrease the leakage current and reduce the trap density in the film.

Experimental

$LaAlO_3$ thin films were deposited in a horizontal gas flow reactor at 300 ^{o}C with the precursors lanthanum tris(*N,N'*-diisopropylformamidinate), trimethylaluminum (TMA) and H_2O. The lanthanum precursor was synthesized by methods similar to those described previously (17). It is the most volatile lanthanum compound known, with a vapor pressure of 82 mTorr at 120 ^{o}C. During the depositions, the lanthanum precursor was heated to 120 ^{o}C in an oven, while TMA and H_2O were kept at ambient temperature. The substrates were n-type Si (100) with resistivity 0.5-1 Ω cm. Before deposition, the substrates were dipped in a 5% aqueous HF solution for 5 sec. to achieve a hydrogen-terminated surface. Each cycle of $LaAlO_3$ consisted of two sub-cycles of La_2O_3 and one sub-cycle of Al_2O_3. A sub-cycle was the sequential dosing of the metal precursor and H_2O with a nitrogen purge following each dose. The pulse ratio of the lanthanum precursor to TMA was 2:1 to obtain a stoichiometry close to $LaAlO_3$. The growth rate was measured to be 2.8 Å/cycle based on thickness measurements from spectroscopic ellipsometry and x-ray reflectivity (XRR). The refractive index of the films was determined by spectroscopic ellipsometry to be between 1.84 and 1.88. To obtain film composition and impurity content, Rutherford backscattering spectroscopy (RBS) was performed on the films deposited on amorphous carbon substrates or Si_3N_4 membrane to increase sensitivity to light elements. The composition was found to be $La_{1.1}Al_{0.9}O_3$. Carbon and nitrogen concentrations were below the detection limit (<1 at. %).

ALD MoN was deposited on the $LaAlO_3$ layers in the same reactor, serving as a capping layer and a gate metal (18). The precursors for the ALD MoN were bis(*tert*-butylimido)bis(dimethylamido)molybdenum and ammonia gas (19). The Mo precursor was kept at 70 ^{o}C in an oven. The deposition temperature for MoN was 300 ^{o}C, at which temperature the growth rate was 0.5 Å/cycle according to thickness measurements by XRR. The stoichiometry is Mo_1N_1 according to RBS and the film was mostly amorphous as deposited (19). The resistivity of MoN was approximately 3000 μΩ cm, measured by a FPP5000 4-point probe.

For electrical analysis, multiple MOS capacitors were made out of MoN/ $LaAlO_3$ stacks on Si. The thickness of the MoN layers was fixed at 20 nm, while the $LaAlO_3$ layers varied in thickness from 5 to 10 nm. Au/Cr was patterned by a lift-off process on the sample to serve as an etch mask and to enhance the conductivity of the top contact for electrical measurement. MoN was then etched by CF_4/Ar reactive ion etching (RIE) through the etch mask to form MOS capacitor structures. The pad area was 10^{-4} cm^2. Backside oxide was etched off by dilute HF, and then Pt/Pd alloy was sputtered on the back to minimize the contact resistance. All of the capacitors then underwent rapid thermal annealing (RTA) at 400 ^{o} C for 4 min in forming gas (5% H_2 + 95% N_2). The leakage current was measured with a Keithley 2400 meter and the C–V curves were taken with a HP 4275A meter in a shielded probe station at room temperature.

Downloaded 06 Feb 2009 to 128.103.93.158. Redistribution subject to ECS license or copyright; see http://www.ecsdl.org/terms_use.jsp

Results and Discussion

The *C-V* curves measured from MOS capacitors with an 8.3 nm thick as-deposited $LaAlO_3$ layer at different frequencies (10 kHz, 100 kHz, 1 MHz) are shown Figure 1 (a).

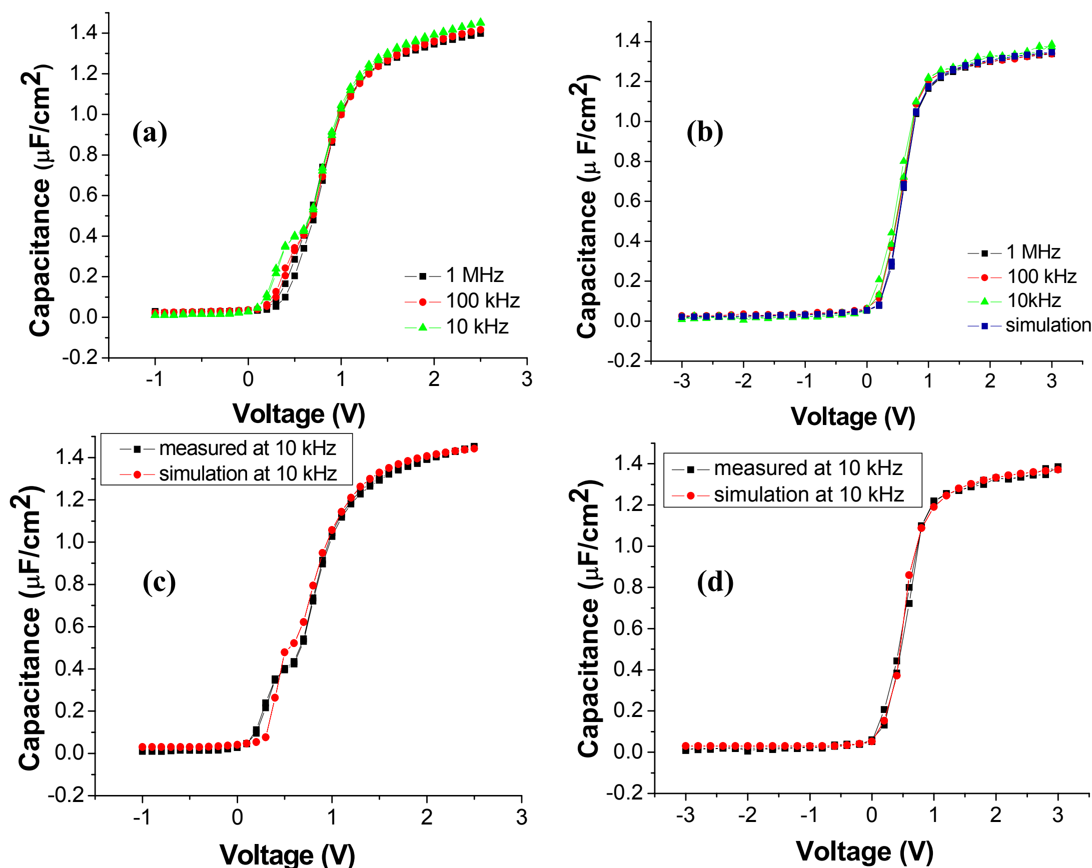

Figure 1. Comparison of *C-V* curves at different frequencies between (a) the as-deposited sample and (b) PDA O_2 treated sample. A simulation curve is at 1 MHz is shown in (b); (c) as-deposited and simulated at 10 kHz; (d) PDA O_2 treated sample and simulated at 10 kHz.

The dielectric constant calculated from the *C-V* curve is around 15, which is lower than the dielectric constant of the bulk material. This may be attributed to the lower density (14) of the $LaAlO_3$ amorphous phase (4.9 g/cm^3 according to the RBS and XRR data) as compared to its crystalline phase (6.5 g/cm^3). Experiments (20) have shown that in the crystalline phase the Al atoms are six-fold coordinated with oxygen, while in the amorphous phase, the coordination number decreases to 4. This decrease of the coordination number may lead to the lower density found in the amorphous phase. The dielectric constant should be lower in the less-dense amorphous phase according to the Clausius-Mossotti relationship (21).

Small humps were found in the midgap region of the *C-V* curves measured at frequencies lower than 100 kHz (Fig. 1a and 1c). In order to find the origin of the humps and try to remove them, we tried *in-situ* post deposition anneal (PDA) at the deposition temperature 300 ^{o}C in O_2 with pressure 1 Torr for 10 min (6×10^8 Langmuir exposure).

Downloaded 06 Feb 2009 to 128.103.93.158. Redistribution subject to ECS license or copyright; see http://www.ecsdl.org/terms_use.jsp

PDA was conducted before the MoN deposition to prevent the oxidation of MoN. As is shown in Figure 1(b), not only are the humps effectively removed at lower frequencies, but also the curve at 1 MHz is less stretched, indicating that fewer traps exist in the film. An equivalent oxide thickness (EOT) of 2.2 nm and flatband voltage of 0.65 V were determined by fitting the measured data by the MISFIT (22) simulation program (including quantum mechanical effects). The measured *C-V* curves showed good agreement with simulation assuming a uniform distribution of electron traps. The estimated trap density in the as-deposited film is 3.5×10^{12} cm^{-2} eV^{-1} by fitting the curve including humps at 10 kHz, while the estimated value for the O_2 treated film is lowered to 6×10^{11} cm^{-2} eV^{-1}, as shown in Figure 1d.

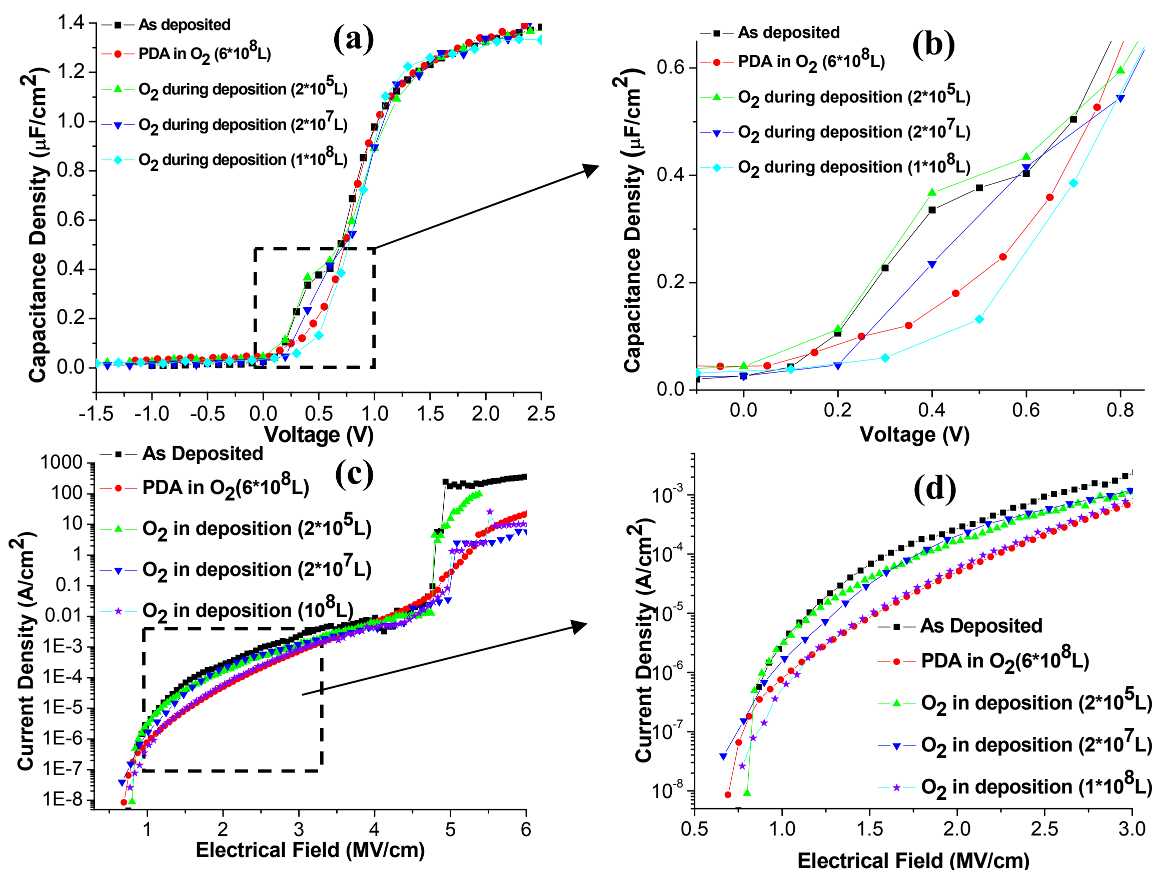

Figure 2. The effect of oxygen exposure on (a) *C-V* curves at 10 kHz and (c) *I-V* curves. The midgap region is zoomed in (b). The middle electrical-field region is zoomed in (d).

Because PDA in O_2 ambient at the deposition temperature was effective, we grew other films that incorporated O_2 exposure during the growth of $LaAlO_3$, rather than after the films were completed. After each complete cycle of $LaAlO_3$, O_2 gas was exposed for various time periods and then purged. Comparing the *C-V* curves measured at 10 kHz, shown in Figure 2 (a), humps were gradually removed as the total exposure of O_2 increased from 2×10^5 Langmuir (L) (by a measured dose of O_2 injected into a continuous flow of N_2) to 1×10^8 L (by O_2 enclosed in the reactor for 5 s without flow). The *I-V* curves in Figure 2(c) also showed gradual improvement. The leakage at 2×10^5 L was similar to the as-deposited sample, but the leakage decreased to that of PDA at an O_2 exposure of 1×10^8 L. None of these treatments decreased the capacitance in the accumulation region, showing that there is no interfacial layer formed after the O_2 treatments.

Downloaded 06 Feb 2009 to 128.103.93.158. Redistribution subject to ECS license or copyright; see http://www.ecsdl.org/terms_use.jsp

I-V curves in Figure 2 (c) and (d) confirmed that PDA in O_2 effectively reduced the leakage current density from 1.1×10^{-4} A/cm^2 to 1.6×10^{-5} A/cm^2 at 1V bias voltage ($|V_G-V_{FB}|$) at EOT = 2.2 nm. For films with EOT = 1.3 nm, the PDA in O_2 reduced the leakage current by a factor of 80, from 80 mA cm^{-2} to 1 mA cm^{-2}.

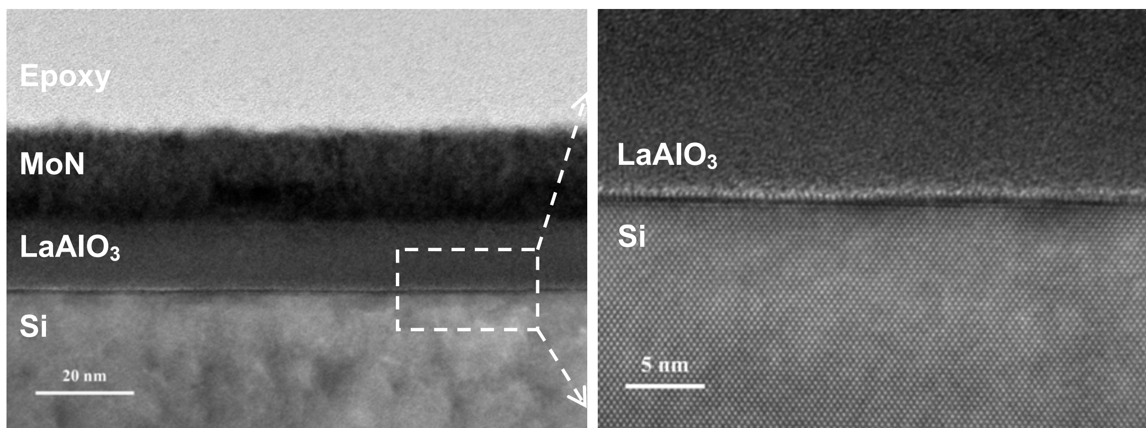

Figure 3. High resolution TEM micrographs of a MoN/$LaAlO_3$ stack on Si. After deposition, the $LaAlO_3$/Si was treated in O_2 at 300 ^{o}C for 10 min, and then the whole stack underwent RTA at 400 ° C for 4 min in forming gas prior to imaging. Both MoN/$LaAlO_3$ and $LaAlO_3$/Si interfaces are sharp and smooth.

Figure 3 shows high resolution cross-sectional transmission electron microscopy (TEM) micrographs of a MoN/$LaAlO_3$ stack on (100) Si. The thicknesses of $LaAlO_3$ and MoN were 12 nm and 20 nm, respectively. $LaAlO_3$/Si was under PDA O_2 treatment at 300 ^{o}C for 10 min, and then the whole stack underwent RTA at 400 ° C for 4 min in forming gas prior to imaging. The images demonstrate that both $LaAlO_3$ and MoN films are uniform. The absence of lattice fringes in the $LaAlO_3$ film is in contrast to the distinct lattice of the Si, confirming that the $LaAlO_3$ film is amorphous. The MoN/$LaAlO_3$ and $LaAlO_3$/Si interfaces are smooth and abrupt. Most importantly, the transition from Si to $LaAlO_3$ is lacking any amorphous low-κ SiO_x interlayer after O_2 annealing which is consistent with the results above from the electrical measurements.

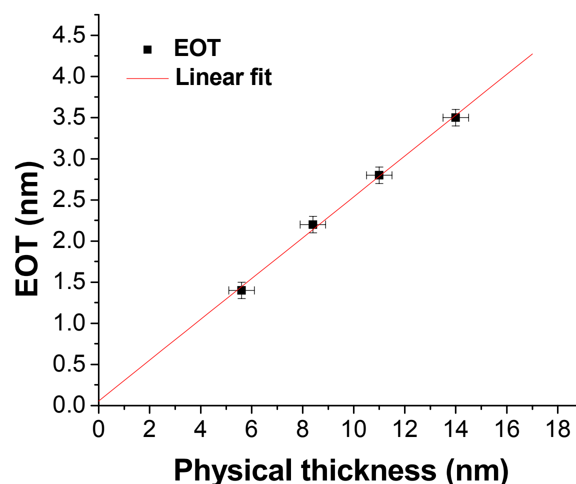

Figure 4. EOT plotted as a function of physical thicknesses of $LaAlO_3$. The intercept from the linear fit is 0.05 ± 0.09 nm and the dielectric constant is 15 ± 1.

Downloaded 06 Feb 2009 to 128.103.93.158. Redistribution subject to ECS license or copyright; see http://www.ecsdl.org/terms_use.jsp

The EOT versus physical thickness (t_{phy}) plot is shown in Figure 4. The y-intercept of the linear fit provides an estimate of the interfacial layer thickness (t_{IL}), and the slope is used to extract the dielectric constant (ε_{LaAlO_3}), as is seen from Eq. (1):

$$EOT = t_{IL} + \frac{\varepsilon_{SiO_2}}{\varepsilon_{LaAlO_3}} \times t_{phy} \qquad [1]$$

The estimated t_{IL} is zero within the experimental error, which provides additional electrical evidence for the idea that there is no low-κ interlayer. The extracted dielectric constant is 15, which agrees with the previous reported value. The results indicate very good scalability of O_2 treated ALD $LaAlO_3$ films.

The effectiveness of O_2 treatments in removing the humps indicates that they are due to oxygen vacancies in the bulk $LaAlO_3$. Guha *et. al.* (23) showed the origin of humps in the *C-V* curve in HfO_2 is positively charged oxygen vacancies. $LaAlO_3$ is also expected to have shallow oxygen vacancies (24). The Frenkel-Poole (FP) conduction mechanism usually fits well with defect-rich ALD HfO_2 films. During FP conduction, trapped charge carriers hop between potential wells that define the trap states, and an applied electric field enhances the hopping state because of the barrier-lowering effect. The current density and the electric field (J-E) characteristics follow the relationship (25):

$$J \sim E \exp[\frac{-q(\Phi_B - \sqrt{qE/\kappa_{dy}\pi})}{kT}] \qquad [2]$$

where κ_{dy} is the dynamic dielectric constant and is the FP trap energy. The electric field in the dielectric was calculated by

$$E = \frac{V_G - V_{FB} - \varphi_s}{t} \qquad [3]$$

where t is the physical thickness of the dielectric, V_G is the voltage being applied to the gate, and φ_s is the silicon substrate band bending. It can be seen from Eq. (2) that the field dependence of the J-E characteristics ln(J/E) vs $E^{1/2}$ should be linear, provided the conduction is dominated by FP hopping.

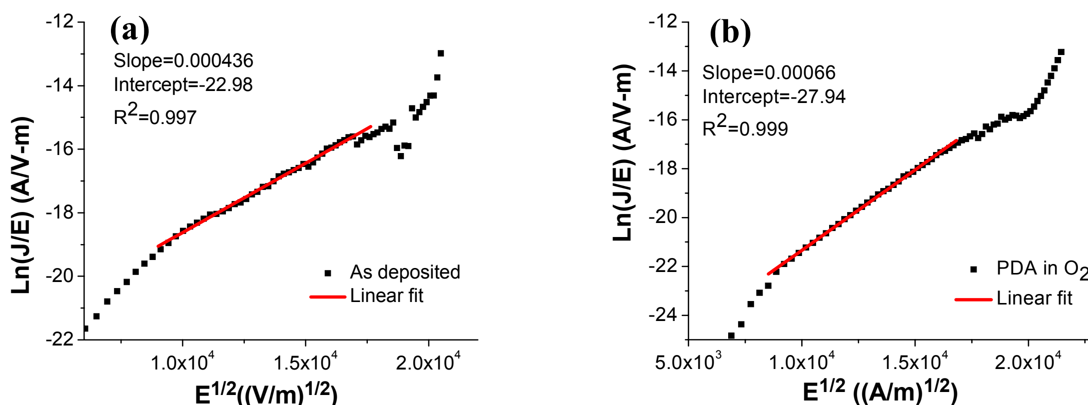

Figure 5. Frenkel-Poole (FP) fitting of the J-E curves measured from (a) as deposited (b) post-deposition-annealed sample at room temperature.

Downloaded 06 Feb 2009 to 128.103.93.158. Redistribution subject to ECS license or copyright; see http://www.ecsdl.org/terms_use.jsp

Figure 5 shows that our data fitted very well using a FP hopping formula from mid- to high field region for both as deposited and post annealed samples. The deviation from the fitted curve in the low-field and high-field regions is believed to result from trap-assisted tunneling and Fowler-Nordheim tunneling (26) respectively, which are excluded from the trap energy calculation. The trap depths of Φ_t and the dynamic dielectric constant κ_{dy} are then extracted from the slopes and the intercepts of the linear fits. The trap depth of Φ_t is 0.69 eV and κ_{dy} is around 2.1 for the PDA sample, while the values for the as deposited one are 0.59 eV and κ_{dy} around 2.6. The extracted values are close to the energy levels of the oxygen vacancies in $LaAlO_3$ calculated in the literature (24). The trap depth of Φ_t is increased from 0.59 eV to 0.69 eV after the O_2 treatment, which might be one of the main reasons why the hump is removed and the leakage current is decreased.

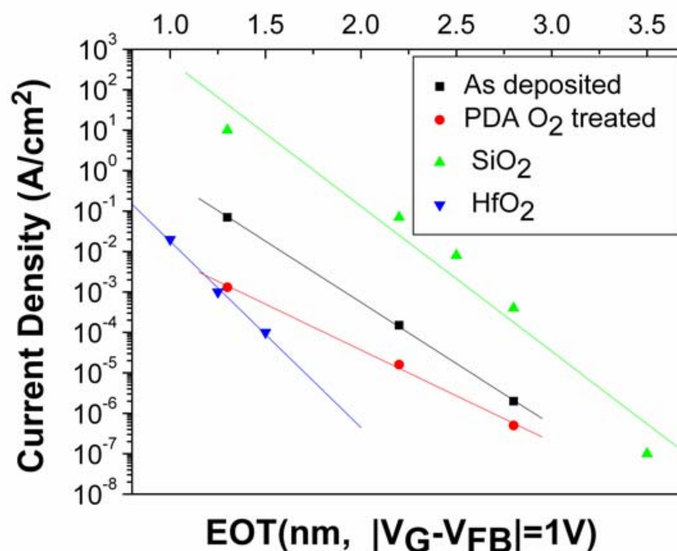

Figure 6. Leakage current density at 1 V of $|V_G-V_{FB}|$ with respect to EOT for $LaAlO_3$ (both as-deposited and samples treated with O_2 after deposition), SiO_2.and HfO_2.

Another important aspect to consider when discussing scalability of a dielectric is how its leakage current density increases with respect to decreasing EOT. Figure 6 shows the leakage current density scaling of both the as-deposited and post annealed $LaAlO_3$ films, compared with that of thermal SiO_2 films (27) and of HfO_2 films (28). The leakage current density of the oxygen post annealed capacitors is about four orders magnitude lower than that of thermal SiO_2 films, and one order magnitude higher than that of HfO_2 films. Lower leakage can be expected if the deposition process is conducted also in the clean room.

In conclusion, we demonstrated that O_2 treatments during deposition or after deposition at 300 ^oC can improve the electrical characteristics of ALD $LaAlO_3$ film. By fitting the J-E curve into the FP formula and comparing the extracted parameters, we proposed a possible reason for the improvement by O_2 treatments.

Acknowledgments

We appreciate Rohm and Haas Electronic Materials for supplying some of the lanthanum precursor.

Downloaded 06 Feb 2009 to 128.103.93.158. Redistribution subject to ECS license or copyright; see http://www.ecsdl.org/terms_use.jsp

References

1. International Technology Roadmap for Semiconductors, http://public.itrs.net/
2. J. Robertson, *Rep. Prog. Phys.,* **69**, 327 (2006).
3. G. D. Wilk, R. M. Wallace, and. J. M. Anthony, *J. Appl. Phys.,* **89**, 5243 (2001).
4. P. W. Peacock and J. Robertson, *J. Appl. Phys.,* **92**, 4712 (2002).
5. K. J. Hubbard and D. G. Schlom, *J. Mater. Res.,* **11**, 2757 (1996).
6. M. Nieminen, M. Putkonen, and L. Niinisto, *Appl. Surf. Sci.,* **174**, 155 (2001).
7. M. Nieminen, T. Sajavaara, E. Rauhala, M. Putkonen, and L. Niinisto, *J. Mater. Chem.,* **11**, 2340 (2001).
8. M. M. Frank, Y. J. Chabal, and G. D. Wilk, *Appl. Phys. Lett.,* **82**, 4758 (2003).
9. A. Stesmans, K. Clémer, V. V. Afanas'ev, L. F. Edge, and D. G. Schlom, *Appl. Phys. Lett.,* **89**, 112121 (2006).
10. L. Miotti, K. P. Bastos, C. Driemeier, V. Edon, M. C. Hugon, and B. Agius, I. J. R. Baum, *Appl. Phys. Lett.,* **87**, 022901 (2005).
11. V. Edon, M. C. Hugon, B. Agius, Miotti, C. Radtke, F. Tatsch, J. J. Ganem, I. Trimaille, and I. J. R. Baum, *Appl. Phys. A,* **83**, 289–293 (2006).
12. V. Edon, M.C. Hugon, B. Agius, C. Cohen, Ch. Cardinaud, C. Eypert, *Thin Solid Films,* **515**, 7782–7789 (2007).
13. M. Wang, W. He, T. P. Ma, L. F. Edge, and D. G. Schlom, *Appl. Phys. Lett.,* **90**, 053502 (2007).
14. T. Busani and R. A. B. Devine, *J. Appl. Phys.,* **96**, 6642 (2004).
15. A. A. Molodyk, I. E. Korsakov, M. A Novojilov, I. E. Graboy, A. R. Kaul, and G. Wahl, *Chem. Vap. Deposition,* **6**, 133 (2000).
16. B. S. Lim, A. Rahtu, P. D. Rouffignac, and R. G. Gordon, *Appl. Phys. Lett.,* **84**, 3957 (2004).
17. B. S. Lim, A. Rahtu, J.-S, Park, and R. G. Gordon, *Inorg. Chem.,* **42**, 7951 (2003).
18. J. Lu, Y.Kuo, S. Chatterjee, and J.-Y. Tewg, *J. Vac. Sci. Technol. B,* **24**, 349-357 (2006).
19. V. Miikkulainen, M. Suvanto, and T. A. Pakkanen, *Chem. Mater.,* **19**, 263(2007).
20. D. Iuga, S. Simon, E. de Boer, and A. P. M. Kentgens, *J. Phys. Chem. B,* **103**, 7591 (1999).
21. I. Bunget and M. Popescu, *Physics of Solid Dielectrics*, p. 16, Elsevier, New York, (1984).
22. G. Apostolopoulos, G. Vellianitis, A. Dimoulas, J. C. Hooker, and T. Conard, *Appl. Phys. Lett.,* **84**, 260 (2004).
23. S. Guha and V. Narayanan, *Phys. Rev. Lett.,* **98,** 196101 (2007).
24. K. Xiong, J. Robertson, and S. J. Clark, *Appl. Phys. Lett.,* **89**, 022907 (2006).
25. S. M. Sze, *Physics of Semiconductor Devices*, p. 402, Wiley Interscience, New York (1981).
26. M. Specht, M. Stadele, S. Jakschik, and U. Schroder, *Appl. Phys. Lett.,* **84**, 3076 (2004).
27. K. H. Kim, D. B. Farmer, J.-S. M. Lehn, P. V. Rao, and R. G. Gordon, *Appl. Phys. Lett.,* **89**, 133512 (2006).
28. S. Kamiyama, T. Miura, and Y. Nara, *Appl. Phys. Lett.,* **87**, 132904 (2005).

Downloaded 06 Feb 2009 to 128.103.93.158. Redistribution subject to ECS license or copyright; see http://www.ecsdl.org/terms_use.jsp